Journal of Power Sources 196 (2011) 9743–9750

Contents lists available at ScienceDirect

Journal of Power Sources

journal homepage: www.elsevier.com/locate/jpowsour

Comparative study of EC/DMC LiTFSI and $LiPF_6$ electrolytes for electrochemical storage

Mouad Dahbi, Fouad Ghamouss, François Tran-Van, Daniel Lemordant, Mériem Anouti*

Université François Rabelais, Laboratoire PCMB (EA 4244), équipe de Chimie-physique des Interfaces et des Milieux Electrolytiques (CIME), Parc de Grandmont, 37200 Tours, France

ARTICLE INFO

Article history:
Received 28 April 2011
Received in revised form 5 July 2011
Accepted 23 July 2011
Available online 30 July 2011

Keywords:
LiTFSI
Activated carbon
Graphite
Asymmetric supercapacitors

ABSTRACT

Lithium bis(trifluoromethane sulfonyl) imide (LiTFSI) salt are potentially a good alternative to $LiPF_6$ since it could both improve the chemical and thermal stability as salt for electrolyte. This work presents a systematic comparative study between $LiPF_6$ and LiTFSI in a mixture of EC/DMC on the basis of some of their physicochemical properties. Transport properties (viscosity and conductivity) are compared at various temperatures from −20 to 80 °C. Using Walden rule, we have demonstrated that LiTFSI 1 M in EC/DMC is more ionic than $LiPF_6$ 1 M in the same binary solvent. Moreover, the electrochemical storage properties of an activated carbon electrode were investigated in EC/DMC mixture containing LiTFSI or $LiPF_6$. The specific capacitance C_s of activated carbon was determined from the Galvanostatic charge–discharge curve between 2 and 3.7 V, at low current densities. The capacitance values were found to be 100 and 90 F g^{-1} respectively for LiTFSI and $LiPF_6$ electrolytes at 2 mA g^{-1}. On the basis of the physicochemical and electrochemical measurements, we have correlated the improvement of the specific capacitance with activated carbon to the increase of the ionicity of the LiTFSI salt in EC/DMC binary system. The drawback concerning the corrosion of aluminium collectors was resolved by adding a few percentage of $LiPF_6$ (1%) in the binary electrolyte. Finally, we have studied the electrochemical behavior of intercalation–deintercalation of lithium in the graphite electrode with EC/DMC + LiTFSI as electrolyte. Results of this study indicate that the realization of asymmetric graphite/activated carbon supercapacitors with LiFTSI based electrolyte is possible.

1. Introduction

Advanced electrochemical systems with high performances are now required for energy storage and electric vehicle applications. For such systems the development of new electrolyte with high conductivity, stability and safety constitute a considerable challenge. For Li-ion systems (batteries, or hybrid supercapacitors) [1–3] mixture of alkylcarbonates with lithium salts are widely used due to their practical operating temperature ranges and their high ionic conductivities [4].

The selection of salts to be dissolved in alkylcarbonates as solvents is decisive in providing highly conductive electrolytes. These salts are often chosen among salts of very strong acids or superacids such as $LiClO_4$, $LiBF_4$, $LiAsF_6$, $LiPF_6$, or CF_3SO_3Li [2,5–7]. Nevertheless, some of them are sometimes dangerous and unstable in contact with highly reactive lithium metal and have a limited stability toward oxidation which restricts the selection of cathode materials. These lithium salts are the result of an acid–base equilibrium with the corresponding Lewis acid, influenced by the electron-donating ability of the solvent and the polarizing nature of Li^+. Nevertheless, chemical toxicity ($LiAsF_6$) and explosion hazards ($LiClO_4$), make these salts unsuitable for a use on a large scale. Special attention has therefore been paid to new lithium salts possessing the previous requirements, i.e., thermal and electrochemical stability.

Usually, electrolyte for a Li-ion battery is composed of lithium hexafluorophosphate ($LiPF_6$) salt dissolved in a mixture of cyclic carbonates like ethylene carbonate (EC) or propylene carbonate (PC) and linear esters such as dimethyl carbonate (DMC), diethyl carbonate (DEC). $LiPF_6$ has been used as the salt in Li-ion batteries for more than a decade because of its unique balance of properties such as good ionic conductivity and ability to passivate aluminium current collector. However, $LiPF_6$ is thermally unstable and decomposes in LiF and PF_5 that can trigger detrimental reactions on the electrode surfaces [3,4]. In addition, $LiPF_6$ and PF_5 react with residual water to form HF [6]. Lithium imide salts are potential alternatives to $LiPF_6$ since they can improve both chemical and thermal stability of the electrolytes. Particularly, lithium bis(trifluoromethane sulfonyl) imide (LiTFSI) salt, is well known to be more stable and safe compared to $LiPF_6$ salt [8]. However, LiTFSI salt is suspected to be corrosive toward Aluminium collector and several studies were focused on this phenomenon [9–12].

* Corresponding author. Tel.: +33 (0)247366951; fax: +33 (0)247367073.
E-mail address: meriem.anouti@univ-tours.fr (M. Anouti).

0378-7753/$ – see front matter © 2011 Elsevier B.V. All rights reserved.
doi:10.1016/j.jpowsour.2011.07.071

Li-ion supercapacitor hybrid systems combining graphite negative electrode and activated carbon (AC) positive electrode have been recently proposed [1,13]. Such system combines the capacitive storage of the AC and the intercalation–deintercalation of lithium in the graphite electrode, leading to an increase of the operating voltage [1]. From this point of view, understanding the comportment of AC electrode in alkyl carbonate + lithium salt is crucial. Recently Beguin et al. have reported an operating voltage (up to 4 V) and a high specific energy (up to 104 Wh kg^{-1}) of this hybrid supercapacitor with EC/DMC 1 M $LiPF_6$ as electrolyte. The authors announced a specific capacitance for the positive AC electrode in EC/DMC 1 M $LiPF_6$ of 86 F g^{-1} [1].

The goal of this study is to establish a systematic comparative study between $LiPF_6$ and LiTFSI salts in a mixture of EC/DMC on the basis of their physicochemical properties and their electrochemical behavior when associated with activated carbons or graphite electrodes.

2. Experimental

2.1. Reagents

Ethylene carbonate (EC) (>99%), dimethyl carbonate (DMC) (>99%), and vinylene carbonate (VC) (>97%), lithium hexafluorophosphate ($LiPF_6$) lithium bis(trifluoromethane sulfone)imide: $LiN(SO_2CF_3)_2$; (LiTFSI) salts were purchased from Aldrich and used without further purification. Electrolyte solutions were prepared in a glove-box filled with argon the residual water was measured by using a Metrohom Karl–Fisher titrator and was found to be below 30 ppm.

3. Measurements

- *Ionic conductivities* were obtained with a Crison (GLP 31) digital multi-frequency conductimeter. The cell constant of conductimetric electrode was determined by using a solution of $LiPF_6$ 1 M in EC/PC/3DMC (σ = 12 mS cm^{-1} at 25 °C, (incertainly: 1%) and the temperature control was ensured by a thermostated bath of PC ($\Delta T \pm 0.2$ °C). Conductivities were measure over temperature range from 20 °C to 80 °C in glove box. From −17 °C to 20 °C measurements have been done in thermostated cell and under Argon flow.
- *Viscosities measurements* were conducted using a TA AR1000 stress rheometer over a temperature range from 20 to 90 °C. The liquid viscosities were determined using conical plan geometry. Typically, the liquid sample volume is 0.5 cm^3.
- *Electrochemical measurement*. Galvanostatic charge–discharge experiments and cyclic voltametry were performed using a Versatile Multichannel Potentiostat (Biologic S.A) piloted by an Ec Lab V9.97 interface. Charge–discharge cycling tests were conducted by using two-electrode configuration. The electrochemical cell was build with a Teflon® Swagelok® system. Graphite or activated carbon disc electrodes coated respectively on copper and aluminium current collector (diameter Ø = 1 cm) were used as working electrode and a Li foil as counter electrode. The potential of the working electrode was recorded with regard to the potential of the Lithium counter electrode. Porous polypropylene membrane (thickness h = 25 μm and pore diameter Ø = 0.2–0.5 μm) filled with the electrolyte solution was used as separator. Electrode materials was supplied by Batscap Corporation and used as received after being dried under vacuum for at least 3 days at 80 °C.

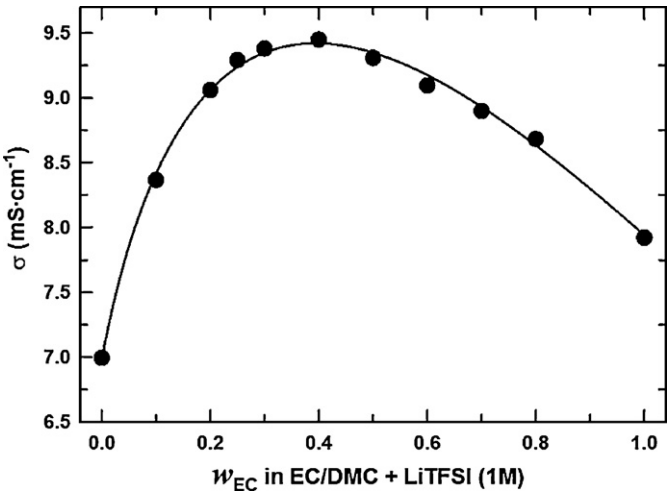

Fig. 1. Variation of conductivities for LiTFSI 1 M in EC/DMC solutions versus weight fraction of EC in solvent mixtures at 298 K.

4. Results and discussion

4.1. Transport properties

4.1.1. Conductivity

Conductivity of the electrolyte plays a key role since internal resistance of the electrochemical system is mostly due to the electrical resistivity of the electrolyte solution. In order to optimize the conductivity of ternary mixture EC/DMC/1 M LiTFSI, we have first optimized the ratio of the two co-solvents in the electrolyte. Fig. 1 shows the variation of the conductivity of EC/DMC + 1 M LiTFSI with different ratios of EC at 25 °C. As it can be seen, the conductivity increases with the raise of weight fraction of EC reaching a maximum for w_{EC} = 0.4 for EC. At this maximum, the conductivity is σ = 9.4 mS cm^{-1}, by comparison at the same concentration and temperature, this value is 10.7 mS cm^{-1} for EC/DMC $LiPF_6$ 1 M electrolyte. The variation of conductivities versus temperature for EC/DMC with both lithium salts is performed in the glove box. Results are presented in Fig. 2, and it clearly indicates that there is no inflection of the conductivities curve for $LiPF_6$ based electrolyte until 80 °C, proving that there is no decomposition of $LiPF_6$ in this controlled atmosphere. The conductivity of the mixture with $LiPF_6$ is higher than the one with LiTFSI in the all range of temperature

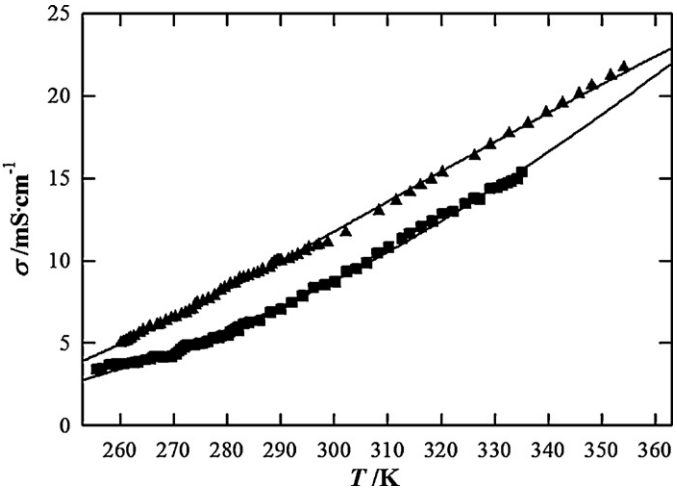

Fig. 2. Variation of conductivities of equimolar mixtures of EC/DMC containing 1 M of: ▲, $LiPF_6$; or ■, LiTFSI as function of temperature.

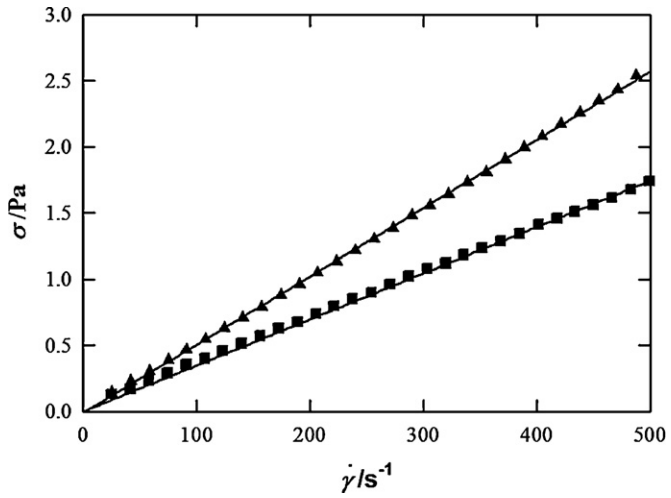

Fig. 3. Flow curves for equimolar mixtures of EC/DMC containing 1 M of: ▲, $LiPF_6$; or ■, LiTFSI at 293.15 K.

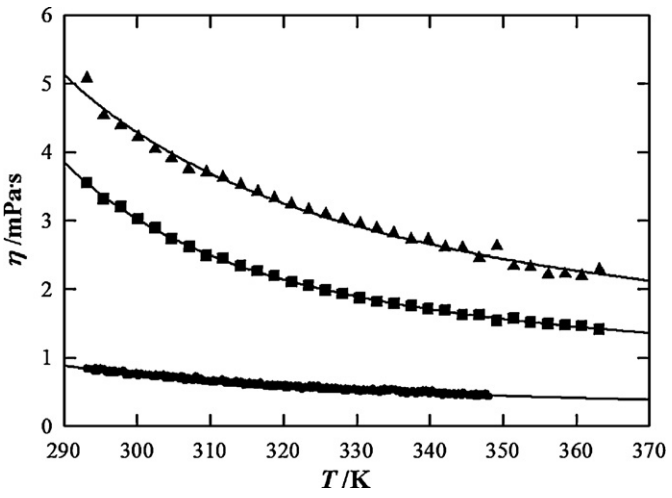

Fig. 4. Variation of viscosities of equimolar mixtures of EC/DMC, ●; containing 1 M of: ▲, $LiPF_6$; or ■, LiTFSI as function of temperature.

investigated. The maximum conductivity in the case of $LiPF_6$ electrolyte is higher by about 30% when compared to LiTFSI electrolytes at 30 °C. This difference is less marked at low temperature (−20 °C, $\Delta\sigma$ = 10%).

4.1.2. Viscosity

Viscosities of the electrolytes are measured by a steady-state flow mode. Typical Newtonian behavior is observed for the liquid sample as indicated by the linear evolution of the shear stress versus the shear rate as shown in Fig. 3. Viscosity does not vary with shear stress or shear rate; viscosity is constant with time of shearing; and stress in fluid immediately falls to zero when shear is stopped.

A series of works described by Matsuda et al. [14] explored the physical properties such as viscosity in mixture of solvents. Using PC/DME as a model system, they investigated the effect of the solvent composition on the viscosity, and correlated these variations with ionic conductivity. They found that the viscosity varied with solvent composition by following an almost linear relation [15]

$$\eta_s = {\eta_1}^{(1-x_2)}{\eta_2}^{x_2} \quad (1)$$

where η_s, η_i, and x_i are the viscosity of the mixture or the pure solvent components (η_1(EC) = 1.85 cP at 40 °C and η_2(DMC) = 0.78 cP at 25 °C) and x_i is the volume fraction of the individual solvent component, respectively. From Fig. 4, the viscosity of a binary system EC/DMC (1/1) (η = 0.88 cP at 25 °C) presents negative deviation from linear relation (2)

$$\eta_{EC/DMC} = \sqrt{\eta_{EC}}\sqrt{\eta_{DMC}} = 1.20 \ \text{cP} \quad (2)$$

After the addition of the $[Li^+X^-]$ (X = PF_6 or TFSI) salt to the EC/DMC mixture, the viscosity of the resulting electrolyte increases from 0.88 cP to 3.9 cP (LiTFI) and 5.1 cP ($LiPF_6$) at 25 °C (Fig. 4). When increases temperature, viscosities of both electrolytes decrease monotonically. The relatively high viscosities of $LiPF_6$ mixture can be attributed to the more solvation of spherical PF_6 anions by solvent molecules. In the case of LiTFSI, lower Van Der Waals interactions occurs and could be probably due to specific repulsion between perfluorinated carbon groups in TFSI with non binding electron of oxygen atom of alkylcarbonate [16,17]. Fig. 5 shows the interdependence of conductivity and viscosity as a function of the temperature. This interdependence is usually evaluated trough the Walden plot (the product ($\sigma\eta$) versus T). As shown in Fig. 5, the Walden product is nearly temperature independent for LiTFSI, although there is a slight increase with temperature for $LiPF_6$. Generally speaking, the increase of $\sigma\eta$ values at a fixed temperature indicates an increase of salt dissociation [18]. Fig. 5 shows that in the all range of temperature, the highest $\sigma\eta$ values were obtained for EC/DMC + 1 M $LiPF_6$ and are attributed to the higher dissociation of $LiPF_6$ compared to LiTFSI in such binary solvent. When the conductivity is completely offset by the viscosity, the Walden product is constant as a function of the temperature. The strong solvation in the case of LiPF6 increase the viscosity despite its greater dissociation compared to LiTFSI and lowers the Walden product. Nevertheless, $LiPF_6$ appears less ionic in the classification of Walden (due to its solvation) compared to LITFSI. Thereby, we can conclude that the dissociation of ions is the dominant factor comparatively to the solvation in the electrolyte in combined conductivity and viscosity parameters.

4.1.3. Fitting Procedure

For the both studied electrolytes, the variations of the conductivity and the viscosity with temperature follow a non-Arhenius behavior as shown in Figs. 6 and 7 for LiX (X = PF_6 and TFSI) 1 M in EC/DMC. However, a Vogel–Tamman–Fulcher (VTF) behavior

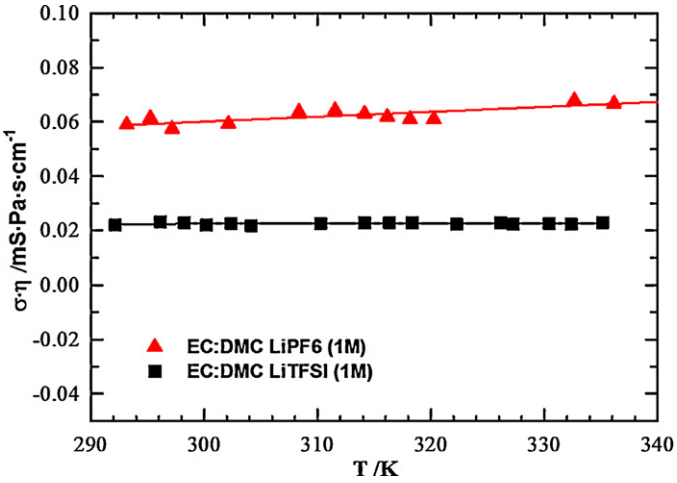

Fig. 5. Walden behavior and interdependence of conductivity and viscosity as a function of temperature for LiTFSI 1 M in EC/DMC and $LiPF_6$ 1 M in EC/DMC solutions.

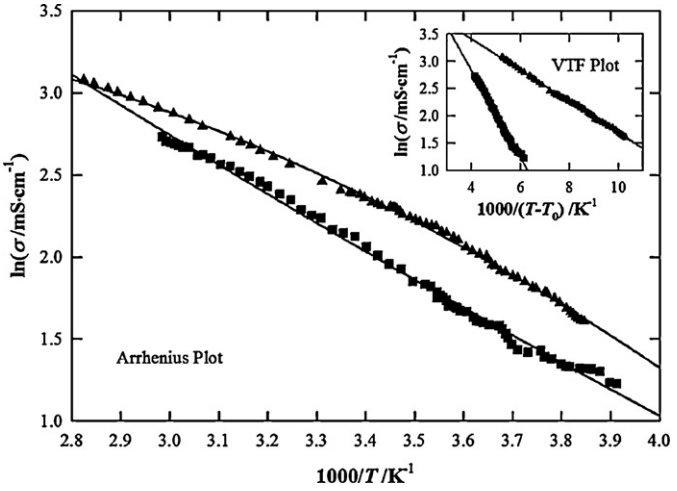

Fig. 6. Arrhenius and VTF variations of conductivity of mixtures of EC/DMC (1/1) containing 1 M of: ▲, $LiPF_6$; or ■, LiTFSI as function of temperature.

according to Eqs. (1) and (2) for viscosities and conductivities are obtained.

$$\eta = \eta_0 \exp\left[\frac{B_1}{(T - T_0)}\right] \quad (3)$$

$$\sigma = \sigma_0 \exp\left[\frac{-B_2}{(T - T_0)}\right] \quad (4)$$

In the VTF equation, B_i is the (pseudo) activation energy, σ_0 is the pre-exponential factor, T_0 is the theoretical glass transition temperature and T is the absolute temperature. For both electrolytes, the T_0 is determined by fitting the temperature-dependent conductivity data to the VTF equation for the best linearity relationship as shows in the inserted graph of Figs. 6 and 7. B_i is determined from the linear slope. The deduced values of T_0 and B_i are listed in Table 1.

From Table 1, it can be found that T_0 (T_0 is the theoretical glass transition temperature, as fitting parameter of VTF), which indirectly reflects the "fragility" [19,20] of the electrolyte systems. Fragility is a novel concept applicable to the study of the behavior of glass-forming liquids. In a simplified picture, fragility is associated with the profile of the potential energy surface and increases with the mean amplitude and variance of the activation barriers. Several approaches have been made to quantify

Table 1
VTF equation parameters for the viscosity as a function of temperature from 293 to 363 K at atmospheric pressure along with the standard deviation δ.

System	η_0/mPa s	B_1/K	T_0/K	δ/mPa s
Viscosity				
EC + DMC	0.118	232.59	174.70	0.02
EC + DMC + $LiPF_6$	0.503	299.07	160.24	0.03
EC + DMC + LiTFSI	0.559	132.68	221.34	0.01
System	σ_0/mS cm^{-1}	B_2/K	T_0/K	δ/mS cm^{-1}
Conductivity				
EC + DMC + $LiPF_6$	97.348	289.79	162.86	0.2
EC + DMC + LiTFSI	50.976	138.66	220.46	0.1

fragility in glassy state physics for example (ii) fragility (F) as the ratio when T_0 and T_g are the "ideal" glass transition temperature and the glass transition temperature, respectively. In other word, conductivities increase very rapidly with temperature when the temperature measurements range is quite far away from T_0 (or T_g).

For LiTFSI in EC/DMC mixture, owing to the relative "strong" interaction between the anion ($TFSI^-$) and cations (Li^+), the lower temperature makes the ionic motion and coulombic interactions more difficult, which results in the reduction of the ionic conductivity of the electrolytes. This phenomenon is accentuated with $LiPF_6$.

4.1.4. Ionicity and Walden rule

The Walden rule [21,22] relates the ionicity represented by the equivalent conductivity Λ to the fluidity η^{-1} of the medium through which the ions move. One way of assessing the ionicity of the electrolyte is to use this Walden diagram. Fig. 8 shows the variation of $\ln(\Lambda)$ versus $\ln(1/\eta)$ at different temperatures for EC/DMC + 1 M lithium salts. The ideal line is obtained on the basis of the ions mobility (determined only by the viscosity of the medium), and number of ions present in the equivalent volume (indicated by salt composition); i.e., all ions contribute equally [23]. The position of the ideal line is established using aqueous KCl solutions at high dilution. We observe in the insert in Fig. 8 that LiTFSI 1 M in EC/DMC is more ionic in the Walden classification, than $LiPF_6$ 1 M in the same binary solvent.

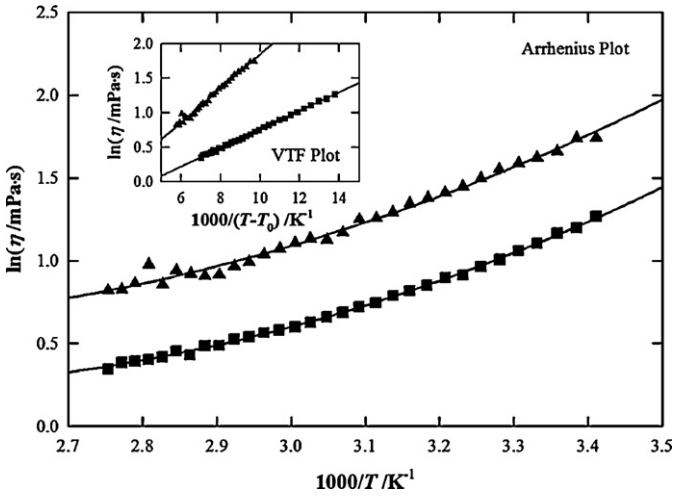

Fig. 7. Arrhenius and VTF variations of conductivity (a) and viscosity (b) of mixtures of EC/DMC (1/1) containing 1 M of: ▲, $LiPF_6$; or ■, LiTFSI as function of temperature.

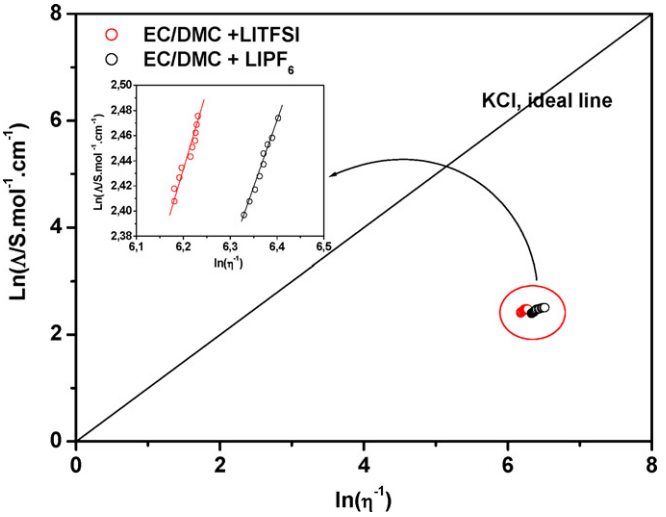

Fig. 8. Walden plots for the EC/DMC (1/1) containing 1 M of: $LiPF_6$ or LiTFSI.

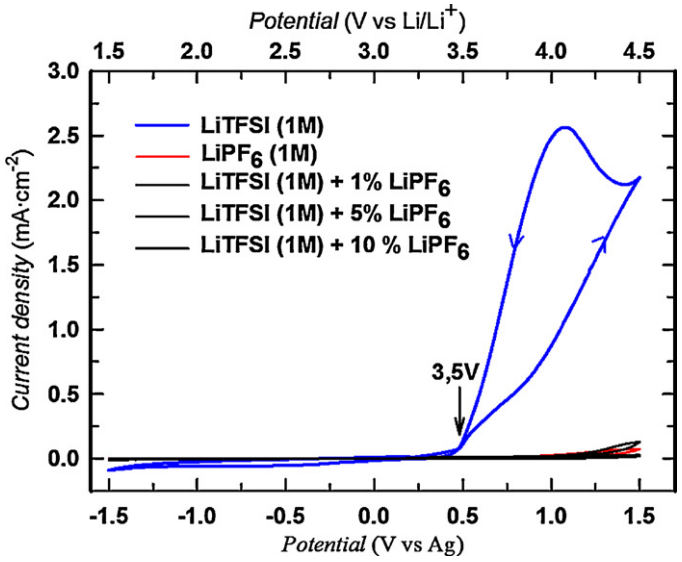

Fig. 9. Cyclic voltammograms of Al electrode in 1.0 M LiTFSI, 1.0 M $LiPF_6$, and 1.0 M LiTFSI containing 1%, 5%, and 10% of $LiPF_6$ in a mixture of EC/DMC (v/v).

4.2. Electrochemical aspects

4.2.1. Comparative anodic behavior of aluminium in LiTFSI and $LiPF_6$ based electrolyte

Aluminium is commonly used as current collector for positive electrode in lithium-ion and EDLC storage systems. The native passive Al_2O_3 layer existing on the metal surface provides protection against corrosion. It is well known that depending on the nature on the electrolyte anions, this passive layer can be broken leading to the corrosion of the Al current collector at high potential. In order to investigate Al behavior in the LiTFSI-based electrolytes, the corrosion behavior of Al was first studied in the LiTFSI and $LiPF_6$ based electrolytes. Then, the impact of $LiPF_6$ as additive on Al passivation was investigated by addition of controlled amount of $LiPF_6$ into pure LiTFSI based electrolyte. Fig. 9 compares the cyclic voltammograms of Al electrode in 1.0 M LiTFSI, 1.0 M $LiPF_6$, and 1.0 M LiTFSI containing 1%, 5%, and 10% of $LiPF_6$ in a mixture of EC/DMC (v/v) in the same condition. In the LiTFSI-based solutions, the voltammogram in the first cycle show a hysteresis loop initiated at about 3.7 V vs. Li/Li^+, with a large irreversible oxidative current peak (up to 2.5 mA cm^{-2}) at about 4.05 V vs Li/Li^+. In the case of $LiPF_6$ (1.0 M) in EC/DMC as expected the initiation potentials of the hysteresis loop move significantly to more anodic side while the peak current sharply decreases. The same behavior is obtained for $LiPF_6$ added from 1% to 10% in 1.0 M LiTFSI based electrolyte. These results suggest that Al passivation would be achieved in the LiTFSI-based electrolytes with small amount of $LiPF_6$ as additive. Fluorides ions (F^-) obtained from the equilibrium equation of decomposition of PF_6^- ion ($PF_6^- \rightarrow PF_5 + F^-$) are responsible to the formation of a passivated layer (fluoroaluminates) on the aluminium collector [12].

4.3. Characterization with half cells

4.3.1. Half cell with a activated carbon as electrode

Keeping in mind that EC/DMC lithium based electrolytes could be appropriate for asymmetric supercapacitors combining graphite negative electrode for lithium insertion–desinsertion process and activated carbon as positive electrode, cyclic voltametry and galvanostatic charge–discharge studies were performed in order to evaluate the capacitive behavior of the activated carbon electrode in LiTFSI and $LiPF_6$ based electrolytes in a half cell configuration and symmetric AC supercapacitor. Fig. 10a shows the cyclic voltammograms of AC obtained at different scan rate between 2 and 3.7 V vs Li/Li^+ in an half cell configuration and Li foil as counter electrode with EC/DMC/1 M LiTFSI as electrolyte. Since the goal of the study is to compare the capacitive behavior of $LiPF_6$ and LiTFSI electrolytes on AC electrodes, the electrochemical window was controlled carefully. Thus, the lower limit of the potential window was fixed at 2 V vs Li/Li^+ to avoid electrolyte decomposition on the carbon positive electrode [1], and its higher limit was first kept at 3.7 V to avoid any current collector corrosion [11,12] especially with LiTFSI. The voltametric response of the single electrode exhibits a pure capacitive behavior with rectangular-shaped profiles. Particularly, the rectangular shape appears to be maintained even at a high rate cycling (20 mV s^{-1}, Fig. 10, black curve) indicating a good rate capability of LiTFSI based electrolyte as well as the classical $LiPF_6$ electrolyte (Fig. 10).

The specific capacitance C_s of the single electrode was determined from the Galvanostatic charge–discharge curve between 2 and 3.7 V (Fig. 10b) by using $C_s = I \times \Delta t/\Delta V \times m$, where m is the weight of the active mass of the CA electrode (4.4 mg), I is the applied current during the galvanostatic discharge, and $\Delta t/dV$ was calculated from calculated the slope of E–t discharge curve.

Calculated capacitances in LiTFSI and $LiPF_6$ EC/DMC electrolytes at different applied current densities are shown in Fig. 11a. At low current densities, the capacitance value was found to be 100 and 90 F g^{-1} respectively for LiTFSI and $LiPF_6$ electrolyte. On the basis of these results one can say that the best capacitances in LiTFSI based electrolyte could be due to the more ionicity of the LiTFSI salt in EC/DMC binary system which was pointed up by the Walden theory in previous section (Section 4.1). Indeed the low solvation TFSI ions favour a better approach near the surface of the external Helmoltz plan, probably due to the more iconicity of LiTFSI salt in EC/DMC mixture according to results obtained from the Walden rule (see Section 4.1.4)

Additionally, capacitance values were rather close to those announced in $TEABF_4$ EC/DMC electrolyte by Egashira et al. [24]. Furthermore, the data of Fig. 11a clearly indicate a decrease of the specific capacitance for both electrolytes when increasing the discharge rate. However, the capacitance drop was slightly more pronounced in the case of LiTFSI as the capacitance loss was evaluated to be 20% between 2 and 10 mA g^{-1} while the capacitance percentage loss was about 10% for $LiPF_6$ electrolyte. One could think that the anion size and by consequence its low diffusivity could be the limiting parameters at fast discharge rate. Indeed, the $TFSI^-$ anion possesses highest hydrodynamic radius [25] which probably affects the kinetic of charge accumulation in the porous structure of the active material.

Fig. 11b shows the evolution of the capacitance of the AC with the temperature at galvanostatic discharge current of 2 A g^{-1}. The specific capacitance increases linearly for both electrolytes when increasing temperature between −10 °C and 60 °C. Beyond this later value, Cs reaches a plateau at 97 F g^{-1} for $LiPF_6$ based electrolyte, while it still increases for the LiTFSI one and reaches 112 F g^{-1} at 80 °C. So, on the basis of these results, we can suggest that LiTFSI should be more appropriate at intermediate temperature beyond 60 °C. This observation was already evoked by several authors and explained by a degradation of the $LiPF_6$ with the generation of HF [26].

4.3.2. Half cell with a graphite electrode

Fig. 12 shows the cyclic voltammograms of Li/Gr half cells in EC/DMC (1 M LiTFSI) electrolyte systems at low scan rate $v = 5\ \mu V\ s^{-1}$. Three quasi-reversible redox transfers (designated in Fig. 13 as "1", "2" and "3"), each characterized by several cathodic and anodic peaks. During the first cathodic potential scan, a large reduction band (see insert in Fig. 12) is observed between 0.7 V and

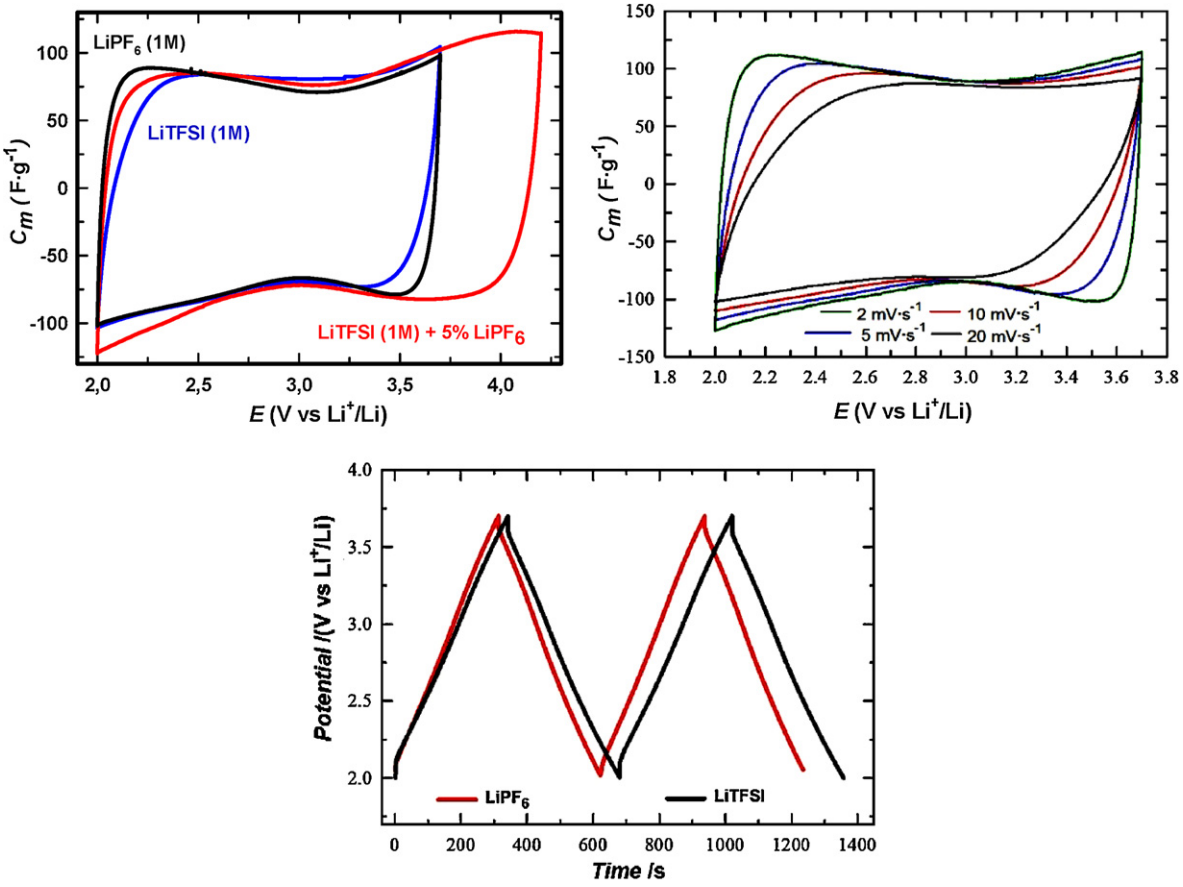

Fig. 10. (a) Cyclic voltammograms at v = 5 (mV s^{-1}) of AC in half cell (AC/Li) in LiTFSI 1 M, $LiPF_6$ 1 M and LiTFSI 1 M + 5% $LiPF_6$ in EC/DMC (1/1). (b) Cyclic voltammograms at v = 2, 5, 10 and 20 (mV s^{-1}) of AC in half cell (AC/Li) in LiTFSI 1 M in EC/DMC (1/1). (c) Galvanostatic charge–discharge curve between 2 and 3.6 V (i = 5 A g^{-1}) of the activated carbon in half cell (AC/Li) using LiTFSI 1 M or $LiPF_6$ 1 M in EC/DMC (1/1).

1. 1 V which can be attributed to the formation of SEI layer, and a broad peak from 0.25 V to 0 V, which could correspond to the Li^+ insertion process. During the reverse anodic process (Fig. 13), two peaks around 0.2 V and 0.25 V (with two shoulders around 0.12 V and 0.17 V) are present, which can be ascribed to the extraction to Li^+ from the graphite electrode (more easy at second stage than the first one). The anodic r current during the second scan is quite well defined with the visualization of three stages of intercalation of lithium in the graphite (1d to 3d), the reduction peak between 0.7 V and 1.1 V disappeared, and three well defined anodic peaks appear (1d to 3d) rises obviously, which signified the increase of cycle efficiency. As described by Levi et al. [27]

The first redox transfer can be ascribed to the transition from phase VIII to IV (peak 1):

$$LiC_{72} + Li \rightleftharpoons 2LiC_{36}$$

The second redox transfer corresponds to the co-existence of phases III and II (peak 2):

$$4LiC_{27} + 5Li \rightleftharpoons 9LiC_{12}$$

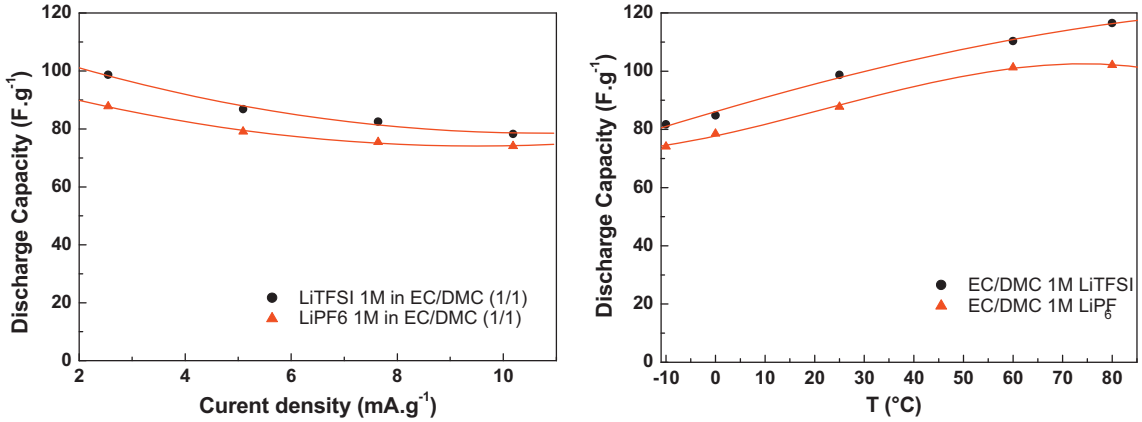

Fig. 11. Comparative capacities in galvanostatic discharge of activated carbon in a half cell (AC/Li) using $LiPF_6$ 1 M in EC/DMC and LiTFSI 1 M in EC/DMC at 2 A g^1 galvanostatic current (a) versus current density, (b) versus temperature.

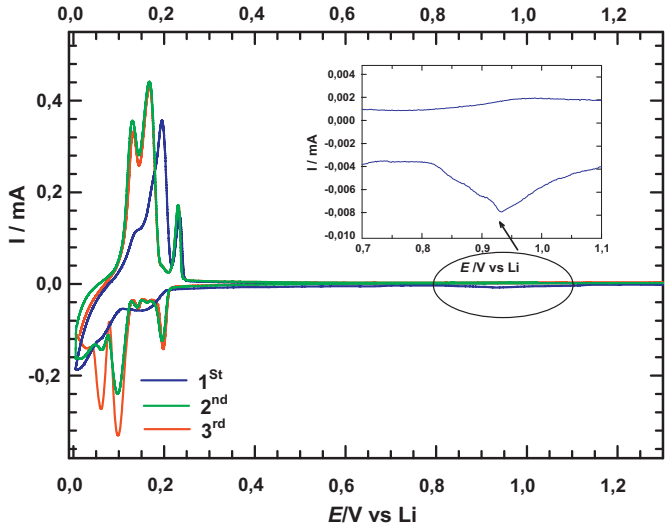

Fig. 12. cyclic voltammograms of Li/Gr half cells in EC/DMC (1 M LiTFSI) electrolyte systems at scan rate $v = 5\ \mu V\ s^{-1}$.

The third redox transfer describes the equilibrium between phases II and I (peak 3):

$$LiC_{12} + Li \rightleftharpoons 2LiC_6$$

The region of potentials between the first (1) and second (2) redox transfer is characterized by a broad plateau of comparatively low current values and contains two additional small peaks which are attributed to intermediate intercalation stage.

The charge ratio between the reduction and oxidation process tends to indicate an increase of the intercalation and de-intercalation process. By comparison with behavior of same cyclic voltammograms of Li/Gr half cells for $LiPF_6$ based electrolyte, the third stage of insertion appear more difficult [27].

The charge/discharge profiles for the LiTFSI and $LiPF_6$-based cell are presented in Fig. 14. The columbic efficiency for the LiTFSI-based cell at the first cycle is 97.3%, which is slightly higher than that 96.6% for the $LiPF_6$-based one, and both of the cells nearly reach 100% efficiency at the second cycle, suggesting that stable electrolyte/electrode interface has been achieved in both the LiTFSI and $LiPF_6$-based electrolytes. Specific capacities of the LiTFSI-based

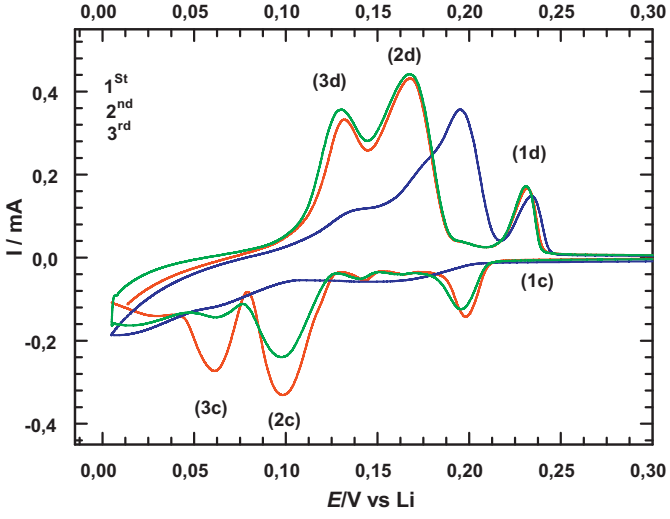

Fig. 13. Li^+ insertion process by cyclic cyclic voltammograms from 0.3 to 0 V/Li of Li/Gr half cells in EC/DMC (1 M LiTFSI) electrolyte systems at scan rate $v = 5\ \mu V\ s^{-1}$.

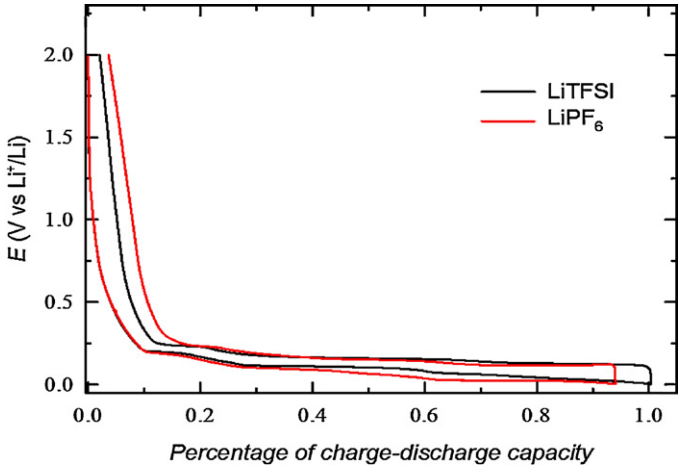

Fig. 14. Cyclability for first cycle at C/10 of graphite/Li Li-ion half cells using 1.0 M LiTFSI and $LiPF_6$ in a mixture of EC/DMC (1:1, v/v).

cell in first cycle is higher than this of the $LiPF_6$-based one, which could be attributed to the lower viscosities of the LiTFSI-based electrolytes, and lower resistance of the SEI layer formed in the LiTFSI-based electrolytes. The data suggest that the LiTFSI salt has good performance in EC/DMC compared to $LiPF_6$ salt.

5. Conclusion

Transport properties (viscosity and conductivity) of both the $LiTFSI^-$ and $LiPF_6^-$ based electrolytes in EC/DMC (1/1, v/v) are compared at various temperatures from −20 to 80 °C. Using Walden rule we have demonstrated that LiTFSI 1 M in EC/DMC is more ionic than $LiPF_6$ 1 M in the same binary solvent. On the basis of the physicochemical and electrochemical measurements, we have correlated the improvement of the specific capacitance of activated carbon to the increase of the ionicity of the LiTFSI salt in EC/DMC binary system. The drawback concerning the corrosion of aluminium collectors in neat LiTFSI salt in EC/DMC was resolved by adding a few percentage of $LiPF_6$ (1%) in the binary electrolyte. Finally Under the same conditions, the performances of both activated carbon/Li and graphite/Li cells are better for LiTFSI than for $LiPF_6$. All these promising performances suggest that LiTFSI in EC/DMC is a promising electrolyte salt for AC/Gr hybrid supercapacitors.

Acknowledgements

This work was supported by the French National Agency for Research. The authors express their gratitude toward Batscap for the supply of the AC electrode materials.

References

[1] V. Khomenko, E. Raymundo-Piñero, F. Béguin, J. Power Sources 177 (2008) 643.
[2] K. Karthikeyan, V. Aravindan, S.B. Lee, I.C. Jang, H.H. Lim, G.J. Park, M. Yoshio, Y.S. Lee, J. Alloy Compd. 504 (2010) 224.
[3] H. Wang, M. Yoshio, A.K. Thapa, H. Nakamura, J. Power Sources 169 (2007) 375.
[4] D. Aurbach, Y. Talyosef, B. Markovsky, E. Markevich, E. Zinigrad, L. Asraf, S.J. Gnanaraj, H.-J. Kim, Electrochim. Acta 50 (2004) 247.
[5] C. Jung, Solid State Ionics 179 (2008) 1717.
[6] Z. Chen, W.Q. Lu, J. Liu, K. Amine, Electrochim. Acta 51 (2006) 3322.
[7] Z. Zhang, X. Chen, F. Li, Y. Lai, J. Li, P. Liu, X. Wang, J. Power Sources 195 (2010) 7397.
[8] A.M. Andersson, M. Herstedt, A.G. Bishop, K. Edström, Electrochim. Acta 47 (2002) 1885.
[9] H.-B. Han, S.-S. Zhou, D.-J. Zhang, S.-W. Feng, L.-F. Li, K. Liu, W.-F. Feng, J. Nie, H. Li, X.-J. Huang, M. Armand, Z.-B. Zhou, J. Power Sources 196 (2011) 3623.
[10] A. Abouimrane, J. Ding, I. Davidson, J. Power Sources 189 (2009) 693.
[11] B. Garcia, M. Armand, J. Power Sources 132 (2004) 206.

[12] J.L. Krause, W. Lamanna, J. Summerfield, M. Engle, G. Korba, R. Loch, R. Atanasoski, J. Power Sources 68 (1997) 320.
[13] H. Wang, M. Yoshio, Electrochem. Commun. 10 (2008) 382.
[14] Y. Matsuda, M. Morita, K. Kosaka, J. Electrochem. Soc. 130 (1983) 101.
[15] M.S. Ding, K. Xu, S.S. Zhang, K. Amine, G.L. Henriksen, T.R. Jow, J. Electrochem. Soc. 148 (2001) A1196.
[16] O. Borodin, G.D. Smith, J. Phys. Chem. B 110 (2006) 6293.
[17] K. Hayamizu, Y. Aihara, S. Arai, B. Garcia, J. Phys. Chem. B 103 (1999) 519.
[18] F. Azeez, P.S. Fedkiw, J. Power Sources 195 (2010) 7627.
[19] R. Richert, C.A. Angell, J. Chem. Phys. 108 (1998) 9016.
[20] C.A. Angell, J. Phys. Chem. Solids 49 (1988) 863.
[21] M. Nakahara, K. Ibuki, J. Phys. Chem. 90 (1986) 3026.
[22] P.Z. Walden, Phys. Chem. (1906) 55207.
[23] J.O.M. Bockris, A.K.N. Reddy, Modern Electrochemistry, Plenum Press, New York, 1998.
[24] M. Egashira, N. Sawada, K. Ueda, N. Yoshimoto, M. Morita, J. Power Sources 195 (2010) 1761.
[25] G. Chen, S. Mukamel, J. Phys. Chem. 100 (1996) 11080.
[26] H. Yang, G.V. Zhuang, P.N. Ross Jr., J. Power Sources 161 (2006) 573.
[27] D.M. Levi, D. Aurbach, J. Electroanal. Chem. 421 (1997) 79.